N_2O_5 Reaction on Submicron Sea Salt Aerosol: Kinetics, Products, and the Effect of Surface Active Organics

Joel A. Thornton* and Jonathan P. D. Abbatt

Department of Chemistry, University of Toronto, Toronto, Ontario, Canada

Received: July 28, 2005; In Final Form: August 31, 2005

The reaction of N_2O_5 on sea salt aerosol is a sink for atmospheric nitrogen oxides and a source of the Cl radical. We present room-temperature measurements of the N_2O_5 loss rate on submicron artificial seawater (ASW) aerosol, performed with an entrained aerosol flow tube coupled to a chemical ionization mass spectrometer, as a function of aerosol phase (aqueous or partially crystalline), liquid water content, and size. We also present an analysis of the product growth kinetics showing that $ClNO_2$ is produced at a rate equal to N_2O_5 loss, with an estimated lower limit yield of 50% at 50% relative humidity (RH). The reaction probability for N_2O_5, $\gamma^{N_2O_5}$, depends strongly on the particle phase, being 0.005 ± 0.004 on partially crystalline ASW aerosol at 30% RH and 0.03 ± 0.008 on aqueous ASW aerosol at 65% RH. At 50% RH, N_2O_5 loss is relatively insensitive to particle size for radii greater than 100 nm, and $\gamma^{N_2O_5}$ displays a statistically insignificant increase from 0.022 to ~0.03 for aqueous ASW aerosol over the RH range of 43−70%. We find that the presence of millimolar levels of hexanoic acid in the aerosol bulk decreases the $\gamma^{N_2O_5}$ at 70% RH by a factor of 3−4 from ~0.025 to 0.008 ± 0.004. This reduction is likely due to the partitioning of hexanoic acid to the gas−aerosol interface at a surface coverage that we estimate to be equivalent to a monolayer. This result is the first evidence that a monolayer coating of aqueous organic surfactant can slow the reactive uptake of atmospheric trace gases to aerosol.

1. Introduction

Heterogeneous reactions of N_2O_5 on aerosol particles constitute an important loss of nitrogen oxide radicals ($NO_x \equiv NO + NO_2$) throughout the troposphere and stratosphere.[1,2] Because NO_x abundance controls the production rate of O_3 in the troposphere, there has been a significant effort to determine $\gamma^{N_2O_5}$, the probability that N_2O_5 will react on an aerosol given a collision with the surface, for a range of aerosol compositions, aerosol size, ambient relative humidity (RH), and temperatures relevant to the troposphere. These studies have shown that, on pH-neutral or mildly acidic aerosol, $\gamma^{N_2O_5}$ increases with RH at low RH, saturates at RH > 50% to a value of ~0.03, and can be orders of magnitude lower on solid particles (see, e.g., Sander et al.[3] and Thornton et al.[4] and references therein). These characteristics imply a dependence on the liquid water content of aqueous aerosol. The reaction can also be inhibited by the presence of aerosol nitrate. This latter effect is important to consider both from an atmospheric perspective and for accurate experimental determination of $\gamma^{N_2O_5}$ since nitrate is the primary reaction product. Experiments that depend on gas−aerosol interaction times of seconds or longer should therefore use initial N_2O_5 concentrations that are as low as possible to avoid a product inhibition in the observed kinetics, and also because atmospheric levels of N_2O_5 are typically less than a few parts per billion by volume (ppbv).

Recently we formulated a reaction mechanism for the hydrolysis of N_2O_5 in mildly acidic or near-neutral aqueous aerosol that incorporates the above characteristics.[4] We proposed that once accommodated into a surface layer at the gas−aerosol interface, $N_2O_{5(aq)}$ reversibly forms a protonated nitric acid intermediate, $[H_2ONO_2]^+$, and dissolved nitrate.

$$N_2O_{5(g)} \rightarrow N_2O_{5(aq)} \qquad \text{(mass accommodation)}$$

$$N_2O_{5(aq)} + H_2O \leftrightarrow H_2ONO_2^+{}_{(aq)} + NO_3^-{}_{(aq)},\ R1_r \qquad (R1)$$

In the absence of other nucleophiles, $[H_2ONO_2]^+$ reacts with H_2O to form $H_3O^+_{(aq)}$ and $HNO_{3(aq)}$ (reaction R2a), which, depending on the aerosol pH either further dissociates to nitrate or evaporates from the particle.

$$H_2ONO_2^+{}_{(aq)} + H_2O \rightarrow H_3O^+_{(aq)} + HNO_{3(aq)} \qquad (R2a)$$

This mechanism accounts for the ability of aerosol nitrate to inhibit the overall reaction rate via reaction $R1_r$, and for a dependence on the availability of liquid water (reaction $R1_f$ and/or reaction R2a). It also allows for the possibility that nucleophiles other than H_2O, such as halide ions, can affect the product yield and reaction rate depending on the rate-limiting step. We suggested that for aqueous organic aerosol with water activity less than 0.4 (RH < 40%), reaction R2a becomes rate limiting, but above RH > 50% either mass accommodation or formation of the intermediate becomes rate limiting.

Sea salt aerosol (SSA), generated by wind and wave action over the oceans, presents a condensed-phase volume for heterogeneous processes in the marine boundary layer. Liquid water content and aerosol size are two characteristics of SSA that might impact $\gamma^{N_2O_5}$. Due to the presence of Mg^{2+} in seawater, SSA contains significant liquid water below the crystallization point of NaCl (RH < 40%) relative to pure NaCl particles.[5,6] This liquid water may enhance the reactivity of N_2O_5

* To whom correspondence should be addressed at Department of Atmospheric Sciences, 408 ATG Building, University of Washington, Seattle, WA 98195. Phone/fax: (206) 543-4010. E-mail: thornton@atmos.washington.edu.

10.1021/jp054183t CCC: $30.25
Published on Web 10/13/2005

on SSA at low relative humidity compared to aerosol composed of pure NaCl which contains only surface adsorbed water,[7,8] making it imperative to study the relative humidity dependence of $\gamma^{N_2O_5}$ on seawater aerosol, not NaCl. The submicron size range dominates the number concentration of SSA. Because the lifetime of aerosol particles increases strongly with decreasing size, submicron SSA likely becomes a more important fraction of the total SSA surface area in air masses that travel away from source regions, making it important to determine whether $\gamma^{N_2O_5}$ depends on SSA size (volume).

The reaction of N_2O_5 on SSA can proceed via two pathways, hydrolysis to nitric acid (via reaction R2a) or reaction with chloride to form nitryl chloride,[9,10] which in the context of the above mechanism would arise via reaction R2b:

$$H_2ONO_2^+{}_{(aq)} + Cl^-{}_{(aq)} \rightarrow ClNO_{2(aq)} + H_2O_{(aq)} \quad \text{(R2b)}$$

Reaction R2a leads to a net loss of 2 NO_x, but the nitryl chloride product of reaction R2b has a low solubility and subsequently evaporates from the particle, where it is photolyzed by sunlight to yield a Cl radical and NO_2 (R3):[11]

$$ClNO_2 + h\nu \rightarrow Cl + NO_2 \quad \text{(R3)}$$

Thus, depending on the branching ratio between reactions R2a and R2b, and on the overall rate, the reaction of N_2O_5 on SSA may be a less efficient NO_x sink compared to other aqueous aerosols. Chlorine activation via reactions R2b and R3 can impact the oxidation pathways of volatile organic compounds because the Cl radical can be ~1000 times more reactive toward gas-phase hydrocarbons than OH.[12] To our knowledge, there are no studies showing the $ClNO_2$ product growth kinetics due to reaction of N_2O_5 on submicron SSA, only the product yield.

Another motivation for this work is that recent experimental and theoretical studies suggest sea salt aerosol may be coated with a layer of organic surfactant material.[13−16] Fatty acids, such as palmitic acid, have been identified as possible surface active components[15−17] while water-soluble organic matter, generally, is associated with surface active material in atmospheric waters.[18] Ellison et al.[13] proposed a general model where products of decaying oceanic biological matter, which would include monocarboxylic acids, are oriented as inverted micelles on the surface of SSA. Such a surfactant coating would significantly alter the gas−aerosol interface and therefore potentially impact the uptake rate of gases to aerosol.

We present measurements of $\gamma^{N_2O_5}$ for submicron sea salt aerosol as a function of relative humidity, mean particle size, and the presence of surface active organic acids. Results were obtained using an entrained aerosol flow tube coupled to a chemical ionization mass spectrometer. Under certain conditions, we could monitor reactant decay and $ClNO_2$ product growth simultaneously. In addition, we believe these are the first studies to provide evidence that trace amounts of surface active organics in the aerosol may alter the net reactive uptake rate of N_2O_5. Given that N_2O_5 likely reacts at the surface and deeper into the aerosol bulk, it can be difficult to differentiate the effects of surface active species if, when added to the aerosol, these species also modify the aerosol bulk. For this reason we chose to equilibrate the aerosol with hexanoic acid vapor, which leads to millimolar levels in the bulk with a monolayer coating at the surface.

2. Experimental Section

The experimental setup to obtain reaction probabilities for N_2O_5 on sea salt aerosol is largely the same as that described in detail previously.[4] We provide only a brief description of the procedures relevant to the current experiment. All experiments were performed at room temperature (~295 K).

2.1. Aerosol Generation and Characterization. Submicron sea salt aerosols were generated by atomizing a dilute solution of artificial seawater (ASW) prepared from deionized water (18 MΩ) and the major ionic components Na^+, K^+, Mg^{2+}, Ca^{2+}, Cl^-, and Br^-, in the ratios described by Kester et al.;[19] we neglected trace amounts of Sr^{2+}. BO_3^-, and F^-. The seawater was diluted with pure water to create atomizing solutions that were 3−12% seawater by volume. Resultant aerosols were entrained in a humidified flow of N_2 and allowed ~10 s to equilibrate with the surrounding RH while being directed to the top of a vertically oriented Pyrex flow tube which acted as the kinetics reactor. The atomizer output is 100% RH. The NaCl in sea salt aerosol crystallizes at RH < 43%.[5] We therefore assumed that the sea salt aerosol was partially crystallized particles containing a residual solution component for RH < 43% and aqueous droplets, supersaturated with respect to dissolved ions, for RH > 43%.

To obtain measurements of aerosol size distributions during the kinetic runs, a portion of the reaction mixture was sampled near the exit of the kinetics flow tube by a scanning mobility particle sizing (SMPS) instrument consisting of a differential mobility analyzer (TSI 3080) and a condensation particle counter (TSI 3010). The ASW aerosol from the atomizer exhibited a broad log−normal distribution with a typical geometric standard deviation of 2.0 and a mean surface-area-weighted particle radius, r_s, ranging from 90 to 150 nm. The latter was varied by atomizing more dilute or more concentrated seawater solutions for smaller or larger particles, respectively.[4] To change the total surface area concentration, S_a, during an experiment, the aerosol number density was adjusted by varying the fraction of the atomizer output mixed into the humidified N_2 carrier. This approach provided S_a between 1×10^{-4} and 3×10^{-3} cm^2 cm^{-3}. During a kinetic run, relative humidity varied less than 2% RH as measured with a commercial hygrometer (VWR), and S_a varied typically less than 5% due to small changes in the atomizer output flow rate. The SMPS was run continuously during kinetics experiments and for 1−2 h prior to the start so that the RH of the sheath flow in the differential mobility analyzer (DMA) reached the RH in the kinetics flow tube. The RH of the flow exiting the DMA was measured after a few experiments and was within a few percent of the desired RH, leading to a negligible impact on the measured surface area due to changes in aerosol water content within the DMA.

2.2. Incorporation of Surface Active Organic Compounds. Monocarboxylic acids that are highly surface active are generally only slightly soluble (parts per million to parts per billion levels or less) in pure water. Furthermore, the smaller acids, while more soluble, have higher vapor pressures and therefore will partition to the gas phase from aerosol generated by atomizing an aqueous solution containing the carboxylic acid. For example, atomizing a dilute seawater solution containing 1×10^{-3} M nonanoic acid would result in aerosol containing ~2×10^{-7} M nonanoic acid assuming Henry's law equilibration between the total available aqueous aerosol volume (~5×10^{-12} L per cm^3 of air) and the gas phase. This estimate is an upper limit due to salting-out effects that likely lower the solubility of nonanoic acid substantially in the highly ionic sea salt aerosol.

Our goal was to test the effect of a monolayer coating of surfactant on $\gamma^{N_2O_5}$. Our approach was to saturate the gas phase with hexanoic acid (HA) and assume that HA partitioned to the aerosol phase according to Henry's law, taking into account

salting-out effects. The humidified sea salt aerosol flow (3−4 slpm) was introduced into a 40 cm long, 6 cm i.d., Pyrex tube through a movable injector (6 mm o.d. stainless steel tube). The Pyrex vessel contained a pool of HA spread along the length. The residence time of aerosol in the tube was 20−25 s. We assume the flow became saturated with HA vapor, which has a vapor pressure of 5.7×10^{-5} atm at room temperature.[20] We do not have direct evidence that the flow was completely saturated, but the setup is similar to our humidification procedure which can bring a 3 slpm flow of dry N_2 to RH > 90%. Additionally, signals detected by the mass spectrometer corresponding to HA ceased to change once the aerosol injector was at least 20 cm from the exit of the saturation vessel. The Henry's law coefficient for HA, H_{HA}, is 1470 M atm^{-1} in pure water,[20] but is much lower in ionic solutions. To determine H_{HA} for the highly ionic sea salt aerosol, we used the method of Setchenow:[21]

$$\log\left(\frac{H^\circ}{H}\right) = \beta[\text{salt}] \qquad (1)$$

where H° is the Henry's law coefficient in pure water, [salt] is the ionic concentration of the solution (mol L^{-1}), and β is the Setchenow salting-out coefficient (L mol^{-1}). The Setchenow coefficient has not been determined for HA, so we followed the approach of Demou and Donaldson,[21] and assumed $\beta = 0.2$ L mol^{-1} for HA. The electrolyte concentration of aqueous sea salt aerosol is a strong function of the ambient RH. At 50% RH, $[Na^+]_{aq} \sim 11.5$ M, while at 70% RH it is ~7 M.[22,23] Thus, $H_{HA} = 5.6$ M atm^{-1} for sea salt aerosol at 50% RH, but increases to 51 M atm^{-1} at 70% RH. The resulting concentrations of HA in the aerosol bulk, assuming Henry's law equilibration with 5.7×10^{-5} atm of HA vapor, are 3×10^{-4} and 3×10^{-3} M at 50% and 70% RH, respectively.

Given that N_2O_5 likely reacts in the aerosol bulk, we chose to use HA, which will form a monolayer at the gas−aerosol interface with only millimolar concentrations in the aerosol bulk. Demou and Donaldson[21] analyzed surface tension measurements to determine surface coverage (molecules cm^{-2}) of HA as a function of bulk HA concentration in aqueous NaCl solutions. This work showed that a $[HA]_{bulk}$ of 3×10^{-3} M corresponded to a surface coverage of $\sim 2.5 \times 10^{14}$ molecules cm^{-2} while a $[HA]_{bulk}$ of 3×10^{-4} M corresponded to a surface coverage less than 5×10^{13} molecules cm^{-2}. A fit to the data using a Langmuir adsorption isotherm implied that a surface coverage of 2×10^{14} molecules cm^{-2} corresponded to a full monolayer at the surface.[21] Thus, in our experiments, we expect ASW aerosol at 70% RH (radius ~200 nm) in equilibrium with HA vapor will have a surface coverage of HA that is equivalent to a monolayer coating, while aerosol at 50% RH will have a submonolayer coverage due to salting-out effects limiting the bulk concentration of HA in the aerosol. For the remainder of the paper, we refer to the HA coverage at 70% RH as a monolayer, but it should be noted that we are unable to determine whether the HA assembles at the gas−aerosol interface as a well-ordered inverted micelle or phase separates into distinct HA pools.

2.3. N_2O_5 Synthesis and Delivery. N_2O_5 was synthesized, stored, and delivered to the kinetics flow tube as described previously.[4] To alter the abundance of N_2O_5 eluting from the storage trap, the trap temperature (typically 200 K) and/or the N_2 carrier flow rate through the trap (1−5 standard cm^{-3} min^{-1}) were/was varied. Resulting N_2O_5 concentrations in the carrier flow are estimates based on an extrapolation of N_2O_5 vapor pressure measurements as a function of temperature,[24,25] and assuming that the flow through the N_2O_5 storage trap became saturated with N_2O_5 vapor.

2.4. Aerosol Kinetics Flow Tube. The aerosol kinetics reactor consisted of a vertically oriented 3 cm i.d., 96 cm long Pyrex tube. A rotary vane pump was used to draw the humidified aerosol flow through a perpendicular sidearm into the top of the flow tube. A critical orifice located at the exit of the flow tube regulated the total flow drawn by the pump to be 1450 standard cm^3 min^{-1} (sccm) at 1 atm and room temperature (300 K). The SMPS drew an additional 350 sccm through a sidearm at the bottom of the flow tube, leading to a total flow velocity through the flow tube of 4.3 cm/s. Our procedure for studying kinetics under conditions of fully developed laminar flow and well-mixed reactants was described previously.[4] A 3 mm o.d. Teflon−PFA tube inserted down the length of a 6 mm o.d. movable stainless steel tube served to inject a 100 sccm flow of N_2O_5 in N_2 axially down the flow tube. After dilution by the humidified aerosol bulk flow, typical initial N_2O_5 concentrations in the reactor ranged from 2×10^{11} molecules cm^{-3} (8 ppbv atm^{-1}) to 7×10^{11} molecules cm^{-3} (30 ppbv atm^{-1}). During an experiment, a small amount of aerosol buildup was observed on the flow tube walls near the 90° entrance point. Measurements of S_a at the top and bottom of the flow tube were consistent to within 5%, as long as the N_2O_5 injector rod was stainless steel, suggesting that aerosol loss to the flow tube wall was a negligible loss of aerosol surface area during a decay. If the injector rod was Pyrex, we observed substantial decreases in aerosol surface area as the injector was pushed further into the flow tube, suggesting preferential loss of aerosol to the Pyrex rod. The inner walls of the flow tube were coated with halocarbon wax, and were washed and dried between each set of experiments.

2.5. N_2O_5 and $ClNO_2$ Detection. N_2O_5 was detected using chemical ionization mass spectrometry (CIMS) with I^- as the reagent ion:

$$I^- + N_2O_5 \rightarrow NO_3^- + INO_2 \qquad (R4)$$

NO_3^- was mass selected and detected at 62 amu. The implementation of this detection scheme, the CIMS apparatus, and sensitivity to N_2O_5 were identical to those described previously.[4] At 50% RH, a typical count rate of 1000 Hz was obtained for 30 ppb N_2O_5 in the absence of aerosol. A persistent background signal was observed at 62 amu under conditions of high aerosol loadings and long reaction times, where N_2O_5 was expected to be completely reacted away. This background scaled with the initial concentration of N_2O_5 in the flow tube. A background value, typically ranging from 10 to 50 Hz, was determined during each experiment at high aerosol loadings and long reaction times. This value was then subtracted from the decay data to produce linear behavior over the entire extent of the decay. The background value was assumed to be constant over the extent of decay. The possible origins of this background have been discussed previously[4] with the most likely explanation being a slow reaction of I^- with HNO_3 and/or conversion of $I^-(HNO_3)$ in the collisional declustering chamber to yield NO_3^-.

During experiments with HA vapor present in the aerosol flow, sensitivity was degraded due to reactions between I^- and HA, and between NO_3^- and HA, as evidenced by detecting ions corresponding to products of reactions R5 and R6

$$I^- + HA \rightarrow I^-(HA) \qquad (R5)$$

$$NO_3^- + HA \rightarrow NO_3^-(HA) \qquad (R6)$$

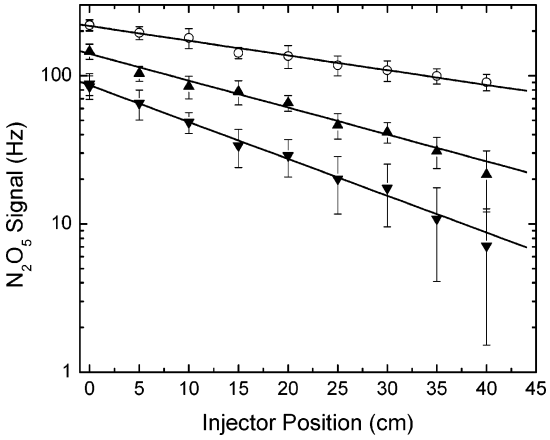

Figure 1. Representative decays of N_2O_5 signal (Hz) plotted on a log scale versus injector position (cm) with 8 ppb N_2O_5 initially present at 50% RH. Error bars represent the 1σ standard deviation of data used to calculate the mean signal at each injector position. A decay in the absence of aerosol (circles, "wall loss") and two decays in the presence of different aerosol surface area concentrations, 0.0005 cm^2 cm^{-3} (up triangles) and 0.0016 cm^2 cm^{-3} (down triangles), are shown.

This degradation of sensitivity led to an initial count rate at 62 amu of 100 Hz for 30 ppb N_2O_5 and 70% RH. The background at 62 amu decreased to a value of less than 10 Hz under these conditions.

An expected product of N_2O_5 reactions on sea salt aerosol is $ClNO_2$ via reaction R2b. We detected an ion signal attributable to ICl^- which we assume is the product of a gas-phase ion−molecule reaction between I^- and $ClNO_2$

$$I^- + ClNO_2 \rightarrow ICl^- + NO_2 \qquad \text{(R7)}$$

Ion signals attributed to ICl^- appeared at *m*/*z* 161 and 163 amu in a constant ratio characteristic of the relative abundance of the stable isotopes ^{35}Cl and ^{37}Cl. These signals were detectable only when N_2O_5 was present in the flow tube, and they responded to changes in N_2O_5 concentration and injector position. No further experiments were conducted to confirm that this signal was in fact due to $ClNO_2$. However, an analogous ion−molecule reaction was observed to occur between I^- and $ClONO_2$ at the gas-collision limit:[26]

$$I^- + ClONO_2 \rightarrow NO_3^- + ICl \qquad \text{(R8)}$$

The electron affinity of NO_3 is greater than that of NO_2;[24] thus we expect that the electron affinity of ICl is between those of NO_2 and NO_3. Based on thermodynamic considerations and recent unpublished work at the University of Washington, it is unlikely that other Cl-containing species, such as HCl or Cl_2, would react with I^- to yield ICl^-.[25] Signals attributable to bromine (Br^- and Br_2^-) were also observed but were too small to analyze (<20 Hz routinely).

3. Results

3.1. N_2O_5 Reaction Probabilities on ASW Aerosol. Figure 1 shows a representative set of N_2O_5 decays obtained during experiments at 50% RH. The average signal at 62 amu is plotted on a log scale versus injector position with and without aerosol present (triangles and circles, respectively). The error bars represent the 1σ deviation of data used in the average, and the signal was corrected for background. The initial N_2O_5 mixing ratio in the flow tube was 8 ppbv; thus experiments with higher N_2O_5 have better precision. The decays appear linear in log space, implying first-order loss of N_2O_5. The slopes of weighted least-squares linear fits to the natural log of the signal versus injector position are converted from units of distance to time by the bulk flow velocity (~4 cm s^{-1}) to yield a first-order rate constant for the loss of N_2O_5 in the flow tube. To obtain the true rate constant for N_2O_5 loss due solely to reaction on aerosol, the observed rate constants are corrected for non plug flow conditions and losses at the flow tube walls using a standard routine[27] described earlier.[4] To capture changes in N_2O_5 loss to the walls during the course of an experiment, observed aerosol decay constants are corrected using wall loss rate constants determined closest in time to the corresponding aerosol decay.

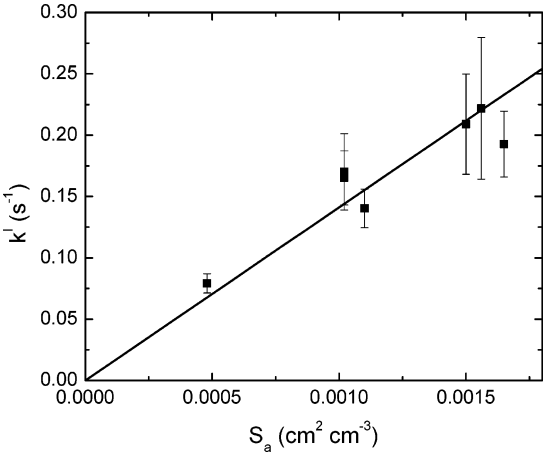

Figure 2. Corrected first-order rate constants, k^I (s^{-1}), for N_2O_5 loss to aerosol plotted versus surface area concentration, S_a (cm^2 cm^{-3}). These particular rate constants were obtained with 8 ppb N_2O_5 at 50% RH (aqueous aerosol), and include the two aerosol decays shown in Figure 1. The error bars are the result of propagating the precisional error in the observed signal through the fitting procedure to determine k^I. The line is an uncertainty weighted least-squares fit to the data forced through the origin.

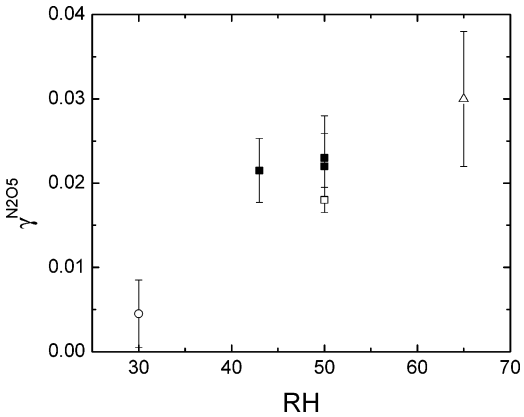

Figure 3. Summary of $\gamma^{N_2O_5}$ determined on aqueous (squares and triangle) and crystalline (open circle, 30% RH) ASW aerosol. The different symbols correspond to different mean particle sizes. See text and Table 1 for details.

The reaction probability, γ_{obs}, is extracted from the first-order rate constants, k^I, using eq 2

$$k^I = \frac{\gamma_{obs}\omega S_a}{4} \qquad (2)$$

where ω is the mean molecular speed of N_2O_5 (cm s^{-1}). Thus, γ_{obs} can be calculated using eq 2 or by determining the slope of a line resulting from a plot of k^I versus S_a as shown in Figure 2. The latter is preferable as the dependence of the kinetics on aerosol surface area is clearly visible. The mean γ_{obs} calculated

TABLE 1: Summary of Experimental Results Listing the Relative Humidity (RH), Mean Surface Area Weighted Particle Radius (r_p), Initial N_2O_5 Mixing Ratio, and Measured N_2O_5 Reaction Probability ($\gamma^{N_2O_5}$)

RH (%)	r_p (nm)	N_2O_5 (ppb)	$\gamma^{N_2O_5}$	note[a]
30	128	25	0.005 ± 0.004	partially crystallized
43	135	30	0.022 ± 0.004	external mixture of aqueous and partially crystallized?
50	134	25	0.022 ± 0.004	aqueous
50	105	25	0.023 ± 0.005	aqueous
50	85	25	0.018 ± 0.002	aqueous
50	132	8	0.025 ± 0.008	aqueous
65	155	25	0.030 ± 0.008	aqueous
70	152	30	0.024 ± 0.005	aqueous
70	152	30	0.008 ± 0.004	aqueous/surfactant

[a] Notes refer to the assumed phase of the aerosol (aqueous or crystalline), and whether surface active organics (i.e., hexanoic acid) were present.

using eq 2 is 0.025 ± 0.008, and that determined from the slope of the line in Figure 2 is 0.023 ± 0.001. The quoted error in the former is the standard deviation of the data used in the mean, and in the latter it is the uncertainty in slope determined by the weighted least-squares fit. The fit in Figure 2 is forced through the origin, but allowing the intercept to vary does not change the results. Gas-phase diffusion can limit the maximum observable reaction probability, and a high reaction probability can alter the gas−aerosol collision frequency from that assumed in eq 2. However, these issues are negligible for the aerosol size ranges and γ_{obs} considered here (<5%), so we assume γ_{obs} is an accurate representation of the true $\gamma^{N_2O_5}$.

Reaction probabilities for N_2O_5 uptake over a range of RH and particle sizes are presented in Figure 3, and summarized in Table 1. The mean surface area weighted particle radius, r_s, ranged from 85 to 165 nm with the points at these two extremes differentiated in Figure 3 by the open square and open triangle, respectively. NaCl crystallizes at <43% RH; hence the reaction probability at 30% RH is relevant only to partially crystallized ASW aerosol, and is thus differentiated by the open circle in Figure 3. For aqueous ASW aerosol, $\gamma^{N_2O_5}$ ranges from 0.018 ± 0.002 to 0.03 ± 0.008, which could reflect both a size dependence (smaller $\gamma^{N_2O_5}$ on smaller particles) and/or a relative humidity dependence (larger $\gamma^{N_2O_5}$ at higher RH). For a constant RH of 50%, the mean r_s was varied from 135 to 85 nm with a corresponding decrease in $\gamma^{N_2O_5}$ from 0.022 ± 0.004 to 0.018 ± 0.002. Thus, the effects of size and RH are fairly small over the ranges examined.

3.2. $ClNO_2$ Production Kinetics. Figure 4 shows the signal at 161 amu, which we attribute to $ClNO_2$, plotted versus injector position for runs with different aerosol surface area concentrations (triangles) and without aerosol (circles). We were only able to examine this chemistry at 50% RH and relatively high N_2O_5 (30 ppbv). The data in Figure 4A were fit to a first-order growth equation using a least-squares method:

$$S^{ClNO_2} = S_\infty^{ClNO_2}(1 - \exp[-k_p x]) \quad (3)$$

where S^{ClNO_2} is the observed signal, x is the injector position, and $S_\infty^{ClNO_2}$ and k_p are variable parameters. The resulting $S_\infty^{ClNO_2}$ values are highly uncertain (±20−75%), making interpretation of these data difficult. The $S_\infty^{ClNO_2}$ values were subtracted from the corresponding signal at each injector position to create a corresponding "decay". An observed rate constant for reaction R2b was then determined from the slope of the natural log versus injector position. This last step is somewhat redundant, as the nonlinear fit produced observed rate constants that were nearly identical to those determined from the corresponding "decay", but this latter method allows visual confirmation that the product growth kinetics are similar to the reactant loss kinetics. Figure 4B shows an example of the resulting decays for "wall" reactions (circles) and for aerosol present (triangles). These two decays are derived from the data presented in Figure 4A corresponding to the same symbols (circles and solid triangles). The squares in Figure 4B show the decay of N_2O_5 in the presence of aerosol observed simultaneously with the $ClNO_2$ data (solid triangles). The slopes of the N_2O_5 and $ClNO_2$ aerosol decays are very similar, but not identical, likely due to the fact that corresponding decays for reaction at the wall are slightly different. The latter were generally more variable for $ClNO_2$ production than for N_2O_5 loss, due in part to the difficulty of accurately determining $S_\infty^{ClNO_2}$.

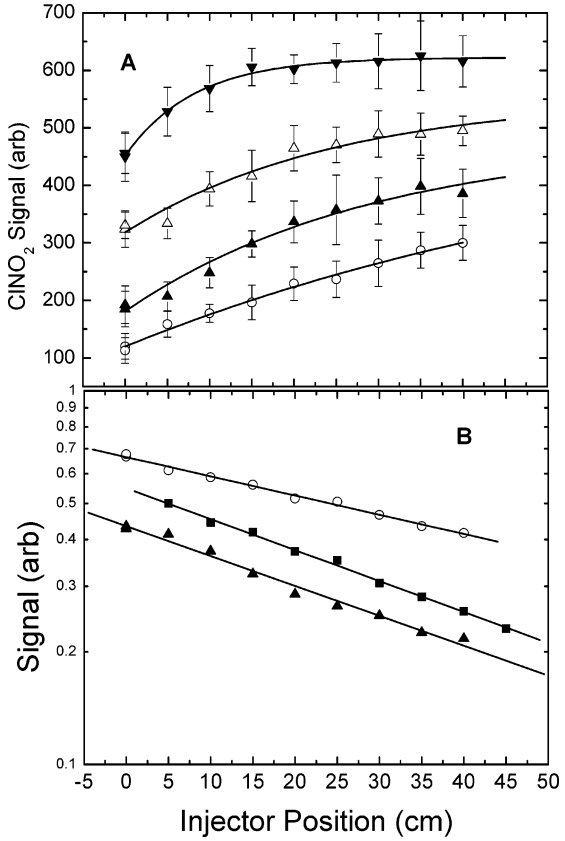

Figure 4. (A) Growth of the signal attributed to $ClNO_2$ plotted versus N_2O_5 injector position obtained with 30 ppb N_2O_5 at 50% RH. Data have been offset for clarity, and different symbols correspond to runs without aerosol (open circle) and runs with aerosol at different S_a values (triangles). The curves are nonlinear least-squares fits to the data using eq 3. (B) Two of these runs as "decays" (circles and triangles). The N_2O_5 decay (squares) obtained simultaneously with the triangle data is shown for comparison.

For a first-order loss of a reactant to several products, the products grow with a rate constant, k_p, that is equal to the first-

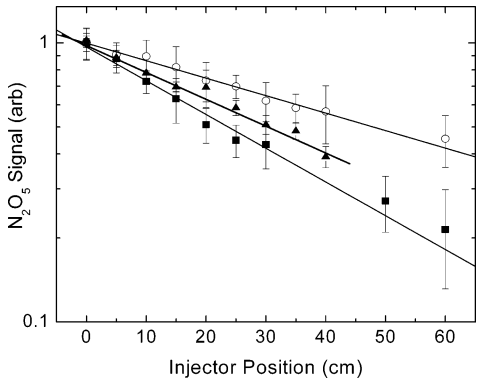

Figure 5. Representative decays of N_2O_5 signal (Hz) plotted on a log scale versus injector position (cm) at 70% RH and with 30 ppb initial N_2O_5. Decays without aerosol (circles), with aerosol (solid squares), and with aerosol containing hexanoic acid (triangles) are shown. Points in this latter decay are the average of four separate decays. Error bars represent the 1σ standard deviation of data used to calculate the mean signal at each injector position.

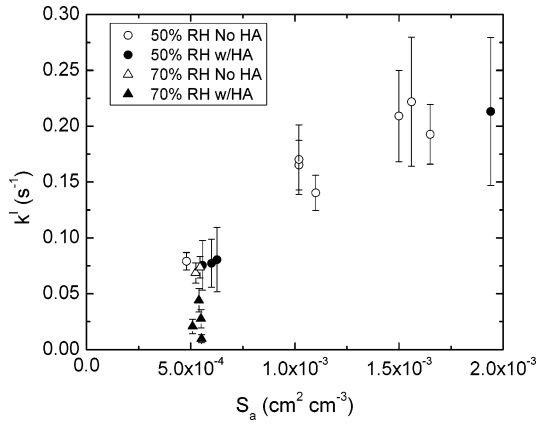

Figure 6. Corrected first-order rate constants, k^I (s^{-1}), obtained for loss of 30 ppb initial N_2O_5 to aerosol at 50% (circles) and 70% RH (triangles) with (solid symbols) and without (open symbols) hexanoic acid (HA) present, plotted versus surface area concentration, S_a (cm^2 cm^{-3}). Error bars are the result of propagating the precisional error in observed signal through the fitting procedure to determine k^I.

order rate constant for reactant loss.[28] Therefore, k_p should equal the rate constant observed for N_2O_5 loss, k^I determined above. The rate constants for $ClNO_2$ growth, k_p, due solely to aerosol, were obtained by subtracting rate constants for wall reaction from those observed with aerosol present. On average k_p was within 90% ± 20% of k^I, but it could be as low as 60% of k^I if the maximum values of $S_\infty^{ClNO_2}$ were used as allowed by their calculated uncertainty. In addition to the uncertainty in $S_\infty^{ClNO_2}$, a highly variable contribution from wall reactions also impacted the calculation of k_p. The quoted range accounts for these issues.

To estimate the product yield for reaction R2b, we took the ratio of the overall increase in ICl^- signal ("$ClNO_2$ produced") to the overall N_2O_5 signal decrease ("N_2O_5 reacted") over the extent of an entire decay. With aerosol present, our product yields are 50 ± 10%, and without aerosol present (i.e., for wall reactions) our product yields are 80 ± 17%. These calculations assume that the detection sensitivity is the same for $ClNO_2$ and N_2O_5. Because N_2O_5 reacts with I^- at the collision limit, it is unlikely that we are more sensitive to $ClNO_2$. Thus, by assuming a 1:1 relationship between $ClNO_2$ signal increase and N_2O_5 decrease, our product yield is likely a lower limit.

3.3. Uptake of N_2O_5 to ASW Aerosol Containing Surface Active Organic Acids. We investigated the effect of surface active organic acids using HA vapor, which we assumed partitions to the bulk aerosol phase according to Henry's law. The Henry's law constant was corrected for a "salting-out" effect using a Setchenow coefficient of 0.2[21] and the relative humidity dependent salt concentration of ASW aerosol (see section 2.2 above). We therefore present an analysis of N_2O_5 decays obtained with aerosol in the presence and absence of HA vapor at both 50% and 70% RH. Figure 5 shows N_2O_5 decays obtained at 70% RH, in the absence of aerosol (open circles), with aerosol present but in the absence of HA (squares), and with both aerosol and HA present (triangles). The latter set of data represent the average of four separate decays obtained with the same aerosol loading. First-order rate constants were derived for each decay as described above.

Rate constants obtained at 70% RH (open and solid triangles) and those obtained for a similar experiment at 50% RH (open and solid circles) are plotted versus aerosol surface area, S_a, in Figure 6. Solid symbols are from experiments with HA vapor present, and open symbols are from those where HA vapor was absent. Assuming eq 2 holds and if the γ is the same for all conditions, all data should lie on the same line. The data obtained at 50% RH lie on the same line, to within experimental precision, corresponding to a $\gamma^{N_2O_5} \sim 0.025$, both with and without HA present, suggesting that there is no significant effect due to HA at 50% RH. The data obtained at 70% RH, on the other hand, display two distinct populations: those without HA (open triangles) lie on a line similar to the 50% RH data, while those with HA present all lie significantly off the line, suggesting a lower $\gamma^{N_2O_5}$ for these aerosols. The latter data are the four runs used to generate the average decay shown in Figure 5. The significant point-to-point variability is due to lowered detection sensitivity and a larger, more variable, wall loss at 70% RH. Using eq 2, a mean $\gamma^{N_2O_5}$ is calculated for data with HA present to be 0.008 ± 0.004 where the quoted error is the 1σ deviation of the data used in the mean.

4. Discussion and Atmospheric Implications

4.1. Reaction Probabilities on Aqueous and Partially Crystallized ASW Aerosols. Our results for $\gamma^{N_2O_5}$ on aqueous ASW aerosol are largely consistent with previous work using ASW or NaCl particles. Given that the compositions of ASW and NaCl aerosols are substantially different, it is interesting that there is little difference in the reactivity of N_2O_5. For RH between 40% and 70%, our $\gamma^{N_2O_5}$ values on ASW aerosol range from 0.02 to 0.03. These data agree well with the value of 0.032 ± 0.002 reported most recently by Behnke et al.[29] for NaCl particles at 60−70% RH, but suggest a slight increase in $\gamma^{N_2O_5}$ with RH. The agreement also suggests that the presence of Br^-, HCO_3^-, Mg^{2+}, and Ca^{2+} in *aqueous* ASW aerosol does not significantly impact the reactivity of N_2O_5 relative to pure NaCl. The largest difference in N_2O_5 reactivity between ASW and NaCl particles appears at RH below the crystallization RH of NaCl, which we address later. Our values for aqueous aerosol are close to, but systematically larger than, 0.018 ± 0.003 reported by Schweitzer et al.[30] for uptake to ~100 μm NaCl droplets between 263 and 278 K. Their work also showed that the N_2O_5 reaction rate was similar on NaBr and NaI droplets, lending further support for the negligible impact of Br^- in ASW aerosol. The proximity of our results to theirs argues against a significant temperature dependence on the uptake process or size dependence for particles with sizes greater than 150 nm. The latter point is somewhat in contrast to the argument presented by Stewart et al.,[7] who observed $\gamma^{N_2O_5}$ values ranging

from 0.006 to 0.014 ± 0.002 on aqueous natural sea salt aerosol with r_s of 108−248 nm. Their lower γ is difficult to explain based on a size dependence as the range of r_s values used in our experiment (85−165 nm) was similar. A more likely explanation is that our initial N_2O_5 concentration was typically 30 ppbv or less, while that of Stewart et al.[7] was 100−700 ppbv, and as they noted, these high levels of N_2O_5 could induce a nitrate inhibition to the reactive uptake.[4,31] Consistent with our previous work, we did not observe a dependence on the initial N_2O_5 concentration if it was less than 30 ppb and if the RH was higher than 40%.[4] While we did not test the impact of N_2O_5 concentrations greater than 30 ppb in the current experiment, we found previously that N_2O_5 levels above ∼100 ppb lowered the observed γ for aqueous malonic acid aerosol at 50% RH.

We present only one result for N_2O_5 uptake to ASW aerosol at 30% RH, i.e., below the crystallization RH of NaCl. Our value of 0.005 ± 0.004 is uncertain due to the difficulty in distinguishing the slow loss to aerosol from wall reactions, but it is in general agreement with previous measurements on "dry" NaCl or ASW particles which range from 3×10^{-4} to 7×10^{-3} (see Hoffman et al.[8] for a recent summary). The large range appears to depend on how hard the particles are dried (e.g., baked at higher temperatures, pumped on overnight, etc.) and the surrounding RH during the measurement, with the lowest values being for pure NaCl crystals. We are in good agreement with the value of $6.8 \times 10^{-3} \pm 0.5 \times 10^{-3}$ reported by Stewart et al.[7] for measurements measured on partially crystallized ASW aerosol at 30% RH. The agreement is somewhat unexpected given that if their results on aqueous aerosol were lower than ours due to the use of higher N_2O_5, the nitrate inhibition (see above) should be most severe for the small aqueous volumes present at 30% RH. While the reason for the differences between our and Stewart et al.'s results for ASW remain uncertain, both measurements of $\gamma^{N_2O_5}$ on partially crystalline ASW are enhanced relative to measurements made with solid NaCl.[7,8] For example, Stewart et al.[7] measured $1.5 \times 10^{-3} \pm 0.5 \times 10^{-3}$ on NaCl aerosol at 30% RH. Hoffman et al.,[8] using a Knudsen cell and a thin layer of partially crystallized ASW particles (RH not reported), inferred 0.03 for γ, which is much larger than their value for solid NaCl particles ($\gamma \sim 0.001$), and it is also larger than our value for partially crystallized ASW aerosol at 30% RH. However, due to the difficulty in analyzing the uptake process for the salt layer, they estimated an uncertainty of a factor of 3.[8]

Our results presented here and those of previous work on aqueous and partially crystallized ASW aerosols support a liquid water dependence to the net reactive uptake of N_2O_5 on pH-neutral or midly acidic particles. Czizco et al.[5,6] found that, below the crystallization RH of NaCl, seawater aerosol exhibited facile exchange of water between the gas and condensed phase while NaCl did not, and attributed this difference to the presence of significant quantities of labile water either as a liquid or as hydrates of Mg^{2+}. While liquid water is also present on or in NaCl particles below 40% RH,[32] the higher reactivity of N_2O_5 on ASW relative to NaCl at 30% RH supports the findings that water present in ASW aerosol is more labile. Thus, N_2O_5 reaction on SSA at RH < 40%, such as inland of the coast, may still be a viable NO_x loss and halogen activation process even though the aerosol would be partially crystalline. However, inland of the coast, N_2O_5 reaction on SSA is probably a minor contribution to NO_x loss overall, depending on the number and properties of non-SSA aerosol.

4.2. $ClNO_2$ Kinetics and Yields. The production of $ClNO_2$ from the reaction of N_2O_5 on sea salt aerosol has been of great interest as it is a means of halogen activation in the polluted marine boundary layer. Although this issue was not a primary focus of the current study, we detected a gas-phase product that we could attribute to $ClNO_2$ under all reaction conditions. Our product growth curves appear to be the only such direct kinetic evidence presented for this system, showing that the $ClNO_2$ growth rate has a rate constant equal to that for N_2O_5 decay at 50% RH. In the context of the mechanism outlined in the Introduction, this result suggests that reaction R2 is not rate-limiting on aqueous ASW aerosol at 50% RH, leaving reaction $R1_f$ or mass accommodation of $N_2O_{5(g)}$ as possible rate-limiting steps. This latter point is supported by the fact that $\gamma^{N_2O_5} \sim 0.03$ at RH > 50% for a range of inorganic and organic aqueous aerosols, such as ASW, ammonium sulfate, and malonic acid.

We derived a $ClNO_2$ product yield estimate of 50 ± 10% at 50% RH. As noted above, our yield estimate is likely a lower limit, and is consistent with 65% determined by Behnke et al.[29] and Karlsson and Ljungstrom[33] on aqueous aerosols at RH > 65% to within stated uncertainties. In this and other studies, the yields measured on aerosol[29,33] are less than those determined on macroscopic films or layers, which generally approach unity.[8] Behnke et al.[29] attribute their lower yields to a loss of $ClNO_2$ on the walls of their Teflon smog chamber. We observe lower limit $ClNO_2$ yields of 80% as N_2O_5 reacts on the walls of our flow tube presumably with ASW aerosol that has impacted on the walls over the course of the experiment. Assuming the $ClNO_2$ yield is actually unity at the wall and that our measured value (80%) is lower due to a lower detection sensitivity for $ClNO_2$ relative to N_2O_5, then our yield with aerosol present increases to 65%, in excellent agreement with that determined by Behnke et al.[29] The agreement suggests little change in the yield of $ClNO_2$ on aqueous aerosol between 50 and 75% RH even though the chloride activity changes by a factor of 3. The reason for higher yields at the flow tube wall is not understood, but several possibilities exist. If the ASW aerosol that deposits on the wall generally crystallizes but retains a thin layer of solution that is high in nitrate and chloride, then reaction channel R2a could be suppressed relative to its importance on aqueous aerosol. This would suggest that the $ClNO_2$ yield should increase on partially crystallized SSA, but we were unable to study the yield under these conditions due to the low total $ClNO_2$ signal that results. Our higher yield at the walls could also be due to additional losses of $ClNO_2$ with aerosol present.

4.3. Effect of Surface Active Organics. We present, to our knowledge, the first experimental evidence that a monolayer coating of organic material on an aerosol will reduce the uptake rate of a trace gas such as N_2O_5. Our confidence in this effect is derived from being able to alter the surface coverage of hexanoic acid by changing only the ambient relative humidity in the flow tube. Additionally, we do not expect the millimolar levels of HA present in the aerosol bulk to affect the reactivity of N_2O_5 in the aerosol bulk because we have measured $\gamma^{N_2O_5} \sim 0.03$ on aqueous malonic acid aerosols at RH > 50%, which is nearly identical to our measurement on pure aqueous ASW not containing HA (0.025−0.03). When approximately a monolayer of HA was predicted to be present on the ASW aerosol, we observed $\gamma^{N_2O_5}$ to be 0.008 ± 0.004, which is about a factor of 3−4 less than that observed without such a monolayer. HA present at less than monolayer coverage did not appear to significantly slow the uptake of N_2O_5. The fact that the effect was so strongly dependent on RH (aerosol ionic strength) is striking, but it is consistent with our rough predictions of HA solubility and bulk−surface partitioning based on surface tension measurements of bulk NaCl solutions containing hexanoic

acid.[21] Our results are related to, but significantly different from, those of Folkers et al.[34] which showed that thick (10−20 nm), multilayer coatings of organic material significantly reduced $\gamma^{N_2O_5}$. Interestingly, we see a similar reduction in $\gamma^{N_2O_5}$ for what can only be a monolayer (∼1 nm) coating.

The presence of a monolayer should only affect either the probability that N_2O_5 will be accommodated at the gas−aerosol interface upon collision, which is represented by α, the mass accommodation coefficient, or the rate of reaction that might occur at the gas−aerosol interface. The observed reaction probability is a convolution of mass accommodation, reaction at the interface, and solubility and reaction in the bulk. The resistor-model framework[35] describes net reactive uptake by assuming these processes are largely decoupled. Neglecting gas phase diffusion limitations, the observed reaction probability in this framework, assuming the surface concentration of N_2O_5 is in equilibrium with the bulk concentration, is given by eq 4:

$$\frac{1}{\gamma^{N_2O_5}} = \frac{1}{\alpha} + \frac{1}{\Gamma_S + \Gamma_B} \quad (4)$$

where Γ_S and Γ_B are the rates of reaction at the interface and in the bulk, respectively, normalized to the gas−aerosol collision frequency. If $\alpha \gg (\Gamma_S + \Gamma_B)$, then $\gamma^{N_2O_5}$ is controlled by the rate of reaction, but if $\alpha \ll (\Gamma_S + \Gamma_B)$, then $\gamma^{N_2O_5}$ is controlled by mass accommodation. There is considerable uncertainty in the value of α for N_2O_5 uptake to aerosol of any composition given that direct measurements, without contribution from reaction, have not been possible. If we assume that $\alpha = 0.1$ for N_2O_5 on ASW aerosol without a monolayer of HA, and if we use our observed $\gamma^{N_2O_5} \sim 0.03$ at 70% RH in eq 4, then uptake to pure ASW aerosol is predicted to be controlled largely by reaction. With a monolayer of HA present on the aerosol, the observed $\gamma^{N_2O_5}$ is 0.008. If bulk reactive processes are the same with and without a coating, then our measurements imply a significant reduction in α and/or Γ_S. For example, in the unlikely event that Γ_S remained constant, α would have to drop by a factor of 10 from 0.1 to ∼0.01. Likely α and Γ_S both change together. Another possibility is that reactive uptake of N_2O_5 is mass accommodation controlled on ASW aerosol at RH > 50%. This notion would imply that $\alpha \sim 0.03-0.05$ on a wide range of inorganic and organic aqueous aerosols (see, e.g., Thornton et al.[4] and references therein) given the similar $\gamma^{N_2O_5}$ values. In this case, the monolayer of organic acid would then reduce α by a factor of 3−6. Presently, there is no clear evidence to distinguish between these possibilities.

4.4. Summary and Conclusions. In summary, $\gamma^{N_2O_5}$ for aqueous submicron sea salt aerosol is likely equal to, or greater than, 0.03 for RH > 50%, as most experimental determinations may have been subject to a nitrate inhibition. The $ClNO_2$ product yield is greater than 50% on submicron aerosol, and it appears there is a reproducible difference in this yield for experiments using aerosol and those using macroscopic films. This difference may be due to a greater importance for N_2O_5 hydrolysis in aerosol, or because the aerosol experiments occur over longer time scales than coated wall flow tube experiments (seconds vs milliseconds), subsequent loss of the $ClNO_2$ product in aerosol may become important. The average radius for accumulation mode sea salt aerosol is ∼1 μm and for coarse mode is ∼10 μm, and thus any size limitations due to measurements on submicron aerosol would also lead $\gamma^{N_2O_5}$ to be larger than 0.03 for particles relevant to the atmosphere. However, given that $\gamma^{N_2O_5}$ has been measured to be about 0.03 for droplets 0.1−100 μm in size, this effect appears to be unimportant. A larger potential effect is whether sea salt or other types of aerosol contain a monolayer (or thicker) coating of organic material. The presence of millimolar levels of hexanoic acid in the aerosol bulk decreases the $\gamma^{N_2O_5}$ at 70% RH by a factor of 3−4. This reduction is likely caused by the partitioning of hexanoic acid to the gas−aerosol interface at a surface coverage that we estimate to be equivalent to a monolayer. This result is the first evidence that a monolayer coating of aqueous organic surfactant can slow the reactive uptake of atmospheric trace gases to aqueous aerosol. Other trace gases would also likely have reduced uptake rates. While there is evidence that surface active organic material is present in sea salt aerosol,[16] it remains to be determined whether this material forms a cohesive, well-ordered monolayer at the gas−aerosol interface. Surfactant coatings may also be present over continental regions on generic sulfate aerosol,[17] suggesting that our observed effect may be globally relevant. Further work is needed in both the laboratory and the field to determine the importance and atmospheric relevance of this effect for other trace gases and surface active organics.

Acknowledgment. This work was funded by the National Science and Engineering Research Council (NSERC) of Canada. J.P.D.A. also acknowledges a Premier's Research Excellence Award (PREA)—Ontario.

References and Notes

(1) Dentener, F. J.; Crutzen, P. J. *J. Geophys. Res. D* **1993**, *98*, 7149−7163.
(2) Hanson, D. R.; Ravishankara, A. R. *J. Geophys. Res. D* **1991**, *96*, 5081−5090.
(3) Sander, S. P.; Friedl, R. R.; DeMore, W. B.; Golden, D. M.; Kurylo, R. F.; Hampson, R. F.; Huie, R. E.; Moortgat, G. K.; Ravishankara, A. R.; Kolb, C. E.; Molina, M. J. *Chemical Kinetics and Photochemical Data for Use in Stratospheric Modeling*; Evaluation Number 13; NASA Jet Propulsion Laboratory, California Institute of Technology: Pasadena, CA, 2000.
(4) Thornton, J. A.; Braban, C. F.; Abbatt, J. P. D. *Phys. Chem. Chem. Phys.* **2003**, *5*, 4593−4603.
(5) Cziczo, D. J.; Abbatt, J. P. D. *J. Phys. Chem. A* **2000**, *104*, 2038−2047.
(6) Cziczo, D. J.; Nowak, J. B.; Hu, J. H.; Abbatt, J. P. D. *J. Geophys. Res. D* **1997**, *102*, 18843−18850.
(7) Stewart, D. J.; Griffiths, P. T.; Cox, R. A. *Atmos. Chem. Phys.* **2004**, *4*, 1381−1388.
(8) Hoffman, R. C.; Gebel, M. E.; Fox, B. S.; Finlayson-Pitts, B. J. *Phys. Chem. Chem. Phys.* **2003**, *5*, 1780−1789.
(9) Behnke, W.; Zetzsch, C. *J. Aerosol Sci.* **1990**, *21*, S229−S232.
(10) Finlayson-Pitts, B. J.; Ezell, M. J.; Pitts, J. N. *Nature* **1989**, *337*, 241−244.
(11) Vogt, R.; Crutzen, P. J.; Sander, R. *Nature* **1996**, *383*, 327−330.
(12) Atkinson, R. *Atmos. Environ., Part A* **1990**, *24*, 1−41.
(13) Ellison, G. B.; Tuck, A. F.; Vaida, V. *J. Geophys. Res. D* **1999**, *104*, 11633−11641.
(14) Latif, M. T.; Brimblecombe, P. *Environ. Sci. Technol.* **2004**, *38*, 6501−6506.
(15) Russell, L. M.; Maria, S. F.; Myneni, S. C. B. *Geophys. Res. Lett.* **2002**, *29*, 1779.
(16) Tervahattu, H.; Juhanoja, J.; Kupiainen, K. *J. Geophys. Res. D* **2002**, *107*, 4319.
(17) Tervahattu, H.; Juhanoja, J.; Vaida, V.; Tuck, A. F.; Niemi, J. V.; Kupiainen, K.; Kulmala, M.; Vehkamaki, H. *J. Geophys. Res. D* **2005**, *110*, D06207.
(18) Decesari, S.; Facchini, M. C.; Mircea, M.; Cavalli, F.; Fuzzi, S. *J. Geophys. Res. D* **2003**, *108*, 4685.
(19) Kester, D. R.; Duedall, I. W.; Connors, D. N.; Pytkowic, R. *Limnol. Oceanogr.* **1967**, *12*, 176−179.
(20) Yaws, C. L. *Yaws' Handbook of Thermodynamic and Physical Properties of Chemical Compounds*; Knovel: Norwich, NY, 2003.
(21) Demou, E.; Donaldson, D. J. *J. Phys. Chem. A* **2002**, *106*, 982−987, and references therein.
(22) Clegg, S. L.; Brimblecombe, P.; Liang, Z.; Chan, C. K. *Aerosol Sci. Technol.* **1997**, *27*, 345−366.
(23) Tang, I. N. *J. Geophys. Res. D* **1997**, *102*, 1883−1893.

(24) *CRC Handbook of Chemistry and Physics*; 71st ed.; Lide, D. R., Ed.; CRC Press: Boca Raton, FL, 1990.
(25) Stull, D. R. *Ind. Eng. Chem.* **1947**, *39*, 517.
(26) Huey, L. G.; Hanson, D. R.; Howard, C. J. *J. Phys. Chem.* **1995**, *99*, 5001−5008.
(27) Brown, R. L. *J. Res. Natl. Bur. Stand.* **1978**, *83*, 1−8.
(28) Steinfeld, J. I.; Francisco, J. S.; Hase, W. L. *Chemical Kinetics and Dynamics*; Prentice Hall: Upper Saddle River, 1998.
(29) Behnke, W.; George, C.; Scheer, V.; Zetzsch, C. *J. Geophys. Res. D* **1997**, *102*, 3795−3804.
(30) Schweitzer, F.; Mirabel, P.; George, C. *J. Phys. Chem. A* **1998**, *102*, 3942−3952.
(31) Mentel, T. F.; Sohn, M.; Wahner, A. *Phys. Chem. Chem. Phys.* **1999**, *1*, 5451−5457.
(32) Weis, D. D.; Ewing, G. E. *J. Geophys. Res. D* **1999**, *104*, 21275−21285.
(33) Karlsson, R.; Ljungstrom, E. *Atmos. Eviron.* **1998**, *32*, 1711−1717.
(34) Folkers, M.; Mentel, T. F. *Geophys. Res. Lett.* **2003**, *30*, 1644.
(35) Hanson, D. R. *J. Phys. Chem. B* **1997**, *101*, 4998−5001.